ADVANCED FUNCTIONAL MATERIALS

DOI: 10.1002/adfm.200700055

The Effects of Multiphase Formation on Strain Relaxation and Magnetization in Multiferroic $BiFeO_3$ Thin Films**

By *Sung Hwan Lim,* Makoto Murakami, Wendy Lynn Sarney, Shen Qiang Ren, Anbusathaiah Varatharajan, Valanoor Nagarajan, Shigehiro Fujino, Manfred Wuttig, Ichiro Takeuchi,* and *Lourdes G. Salamanca-Riba**

Multiferroic epitaxial Bi-Fe-O thin films of different thicknesses (15–500 nm) were grown on $SrTiO_3$ (001) substrates by pulsed laser deposition under various oxygen partial pressures to investigate the microstructural evolution in the Bi-Fe-O system and its effect on misfit strain relaxation and on the magnetic properties of the films. Films grown at low oxygen partial pressure show the canted antiferromagnetic phase α-Fe_2O_3 embedded in a matrix of $BiFeO_3$. The ferromagnetic phase, γ-Fe_2O_3 is found to precipitate inside the α-Fe_2O_3 grains. The formation of these phases changes the magnetic properties of the films and the misfit strain relaxation mechanism. The multiphase films exhibit both highly strained and fully relaxed $BiFeO_3$ regions in the same film. The magnetization in the multiphase Bi-Fe-O films is controlled by the presence of the γ-Fe_2O_3 phase rather than heteroepitaxial strain as it is the case in pure single phase $BiFeO_3$. Also, our results show that this unique accommodation of misfit strain by the formation of α-Fe_2O_3 gives rise to significant enhancement of the piezo electric properties of $BiFeO_3$.

1. Introduction

Multiferroic materials simultaneously display ferroelectric and ferromagnetic properties in the same phase. [1] In the 1960s to 1970s, these materials were first investigated to understand the magnetoelectric (ME) coupling effect.[2,3] Recently, there is increased interest in multiferroic materials because of their potential applications in novel devices using the magnetoelectric effects including switching of the electric polarization controlled by an applied magnetic field.[4–6] Very few intrinsic multiferroic compounds such as $HoMnO_3$ and $TbMn_2O_5$ exist in nature or have been synthesized. Furthermore, these materials exhibit the ME coupling at low temperatures.[6–9]

$BiFeO_3$ has attracted great attention because it is multiferroic well above room temperature.[10,11] However, the small magnetization and narrow growth window of $BiFeO_3$ impede its use in practical applications. To enhance the magnetic and ferroelectric properties of $BiFeO_3$, chemical modification, and controlled stress through growth of heteroepitaxial films and variation in thickness have been attempted with varying degrees of success.[5,12,13] In Bi-Fe-O, however, there are several phases of different structures, compositions, and electrical and magnetic properties which can co-exist. The presence of these phases can substantially affect the electrical and magnetic properties of the overall material. There has been a report on the coexistence of $BiFeO_3$ and γ-Fe_2O_3 phases in Bi-Fe-O films grown by pulsed laser deposition (PLD).[14] We have recently reported on the coexistence of $BiFeO_3$ and Fe_2O_3 phases (α and γ) with a systematically varying degree of mixture controlled by the oxygen partial pressure during deposition.[15] In the present work, we investigate the microstructural evolution in Bi-Fe-O films which form nanocomposites consisting of more than one phase when the thickness of the film is changed. We focus on characterization of the secondary phases and the effects of these phases on the relaxation of the lattice misfit strain and the magnetic properties of the overall films.

Figure 1a shows X-ray diffraction (XRD) spectra obtained from films of different thicknesses, t, grown at an oxygen partial pressure of 5 mTorr. Diffraction was performed using the ω-scan mode, and the intensities were integrated in χ between 85 and 95 degrees. The corresponding TEM cross-sectional images of some of the films are shown in Figure 1b. In our previous report,[15] thin films of pure $BiFeO_3$, which has a perov-

---

[*] S.-H. Lim, Prof. L. G. Salamanca-Riba, Dr. M. Murakami, S. Q. Ren, S. Fujino, Prof. M. Wuttig, Prof. I. Takeuchi
Department of Materials Science and Engineering
University of Maryland
College Park, Maryland 20742 (USA)
E-mail: shlim@umd.edu; riba@umd.edu

Dr. W. L. Sarney
Sensors & Electron Devices Directorate
U.S. Army Research Laboratory
Adelphi, Maryland 20783-1197 (USA)

A. Varatharajan, Dr. V. Nagarajan
School of Materials Science and Engineering
University of New South Wales
Sydney NSW 2052 (Australia)

[**] This work was supported by NSF MRSEC DMR-00-0520471, ONR N000140110761, ONR N000140410085, NSF DMR 0094265 (CAREER), NSF DMR 0231291 and NSF 0095166. It was also supported by W. M. Keck Foundation and Provincia Autonoma di Trento, Italy, under the Microcombi project. We acknowledge the use of the TEMs in the Nanoscale Imaging Spectroscopy and Properties (NISP) laboratory at the University of Maryland. The NISP laboratory is a Shared Experimental Facility of our NSF MRSEC.

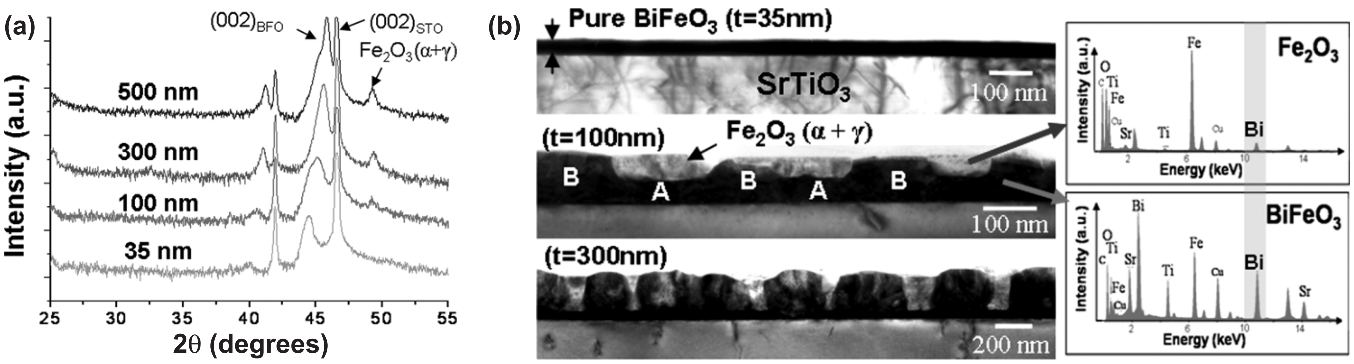

Figure 1. a) X-ray diffraction spectra (in log scale) and b) TEM cross-sectional images (left) and EDS spectra (right) of Bi-Fe-O films grown at 5 mTorr with different thickness. Nucleation of impurity phases starts at ~50 nm. The intensity of the peak labeled Fe_2O_3 in (a) corresponding to the impurity phase increases with increasing film thickness.

skite structure in bulk with $a = 0.395$ nm,[16] grown at 20 mTorr and higher oxygen partial pressure showed a monoclinically distorted (by about 0.5°) tetragonal structure with the lattice constants, $a = 0.394$ nm, $c = 0.398$ nm. In the present work, the 35 nm thick film grown at 5 mTorr oxygen partial pressure shows the pure epitaxial $BiFeO_3$ phase with the [001] orientation and a slightly larger lattice parameter ($c = 0.407$ nm) than that of the pure 300 nm thick $BiFeO_3$ film grown at 20 mTorr. As the film thickness increases, the intensity of the (002) diffraction peaks of the $BiFeO_3$ increases, and the peak shifts to a higher 2θ angle (see Fig. 1a). This indicates that the out-of-plane lattice parameters of $BiFeO_3$ decreases with increasing thickness. We also observed peaks corresponding to the (024) plane of the α-Fe_2O_3 phase and the (240) plane of the γ-Fe_2O_3 phase. The α-Fe_2O_3 phase has a rhombohedral crystal structure (space group: R-3c) with lattice constants of $a = b = 0.505$ nm, $c = 1.319$ nm, and the γ-Fe_2O_3 phase has the cubic (or inverse spinel) crystal structure that belongs to the space group P4132 (or *Fd-3m*) with lattice parameters $a = 0.83515$ nm.[17] The intensity of the peaks corresponding to α- and γ-Fe_2O_3 in Figure 1a increases with increasing film thickness.

From the TEM cross-sectional images of films with different thickness shown in Figure 1b, we can see that the secondary phase, α-Fe_2O_3, forms in the surface region of films with thickness of 50 nm, which grows to the surface of the film with continued deposition. The EDS spectra in Figure 1b obtained from the bright and dark columns of the film confirmed the chemical composition of the separated phases. The EDS spectrum from the bright columns shows little bismuth contents (5.5 at %), and the ratio between iron (38.5 at %) and oxygen (56 at %) is 1:1.45, which is consistent with Fe_2O_3. The EDS spectrum from the dark columns, shows a 1:1.1 ratio between bismuth (24 at %) and iron (26.3 at %), which is consistent with $BiFeO_3$.

The magnified TEM images from cross-sectional and plan-view specimens in Figure 2a show that the γ-Fe_2O_3 phase forms precipitates with a plate-like shape embedded in the α-Fe_2O_3 regions. From indexing the SAD patterns (see Fig. 2b), we obtained the following preferred in-plane epitaxial relations among $BiFeO_3$, α-Fe_2O_3, and γ-Fe_2O_3; $[100]_{BiFeO_3}//[102]_\alpha//[120]_\gamma$, and $[010]_{BiFeO_3}//[1–12]_\alpha//[2–1–1]_\gamma$. The γ-Fe_2O_3 also showed different orientations with respect to $BiFeO_3$ and α-Fe_2O_3 in other areas of the sample. Typically, Fe_2O_3 has two different crystal structures. One is a spinel structure (maghemite, γ-Fe_2O_3) and the other is a corundum structure (hematite, α-Fe_2O_3). In bulk, it is known that there is an irreversible transformation from γ-Fe_2O_3 to α-Fe_2O_3 occurring at temperatures above 400 °C via restacking of the oxygen layers and displacement of the Fe ions located in the interstices rather than recrystallization.[18] This transformation occurs on the close-packed planes of α- and γ-Fe_2O_3 without diffusion, and thus the crystal orientation relationship between α- and γ-Fe_2O_3 in the bulk was reported as $(0001)_\alpha//(111)_\gamma$, $[01–10]_\alpha//[1–10]_\gamma$.[17,19,20] In our experiments, however, we observed the co-

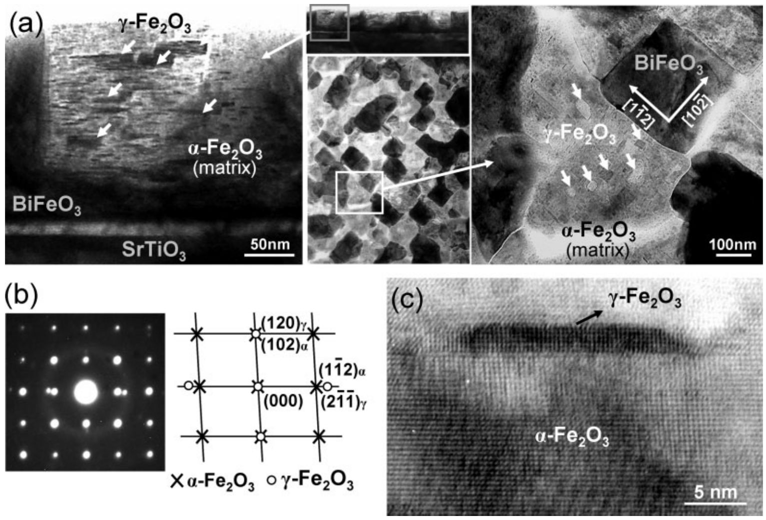

Figure 2. TEM bright field images and SAD pattern of bismuth iron oxide thin films fabricated on (001) $SrTiO_3$ substrates. a) Cross-section (left) and plan-view (right) images showing γ-Fe_2O_3 precipitates and b) SAD pattern and corresponding schematic of α-Fe_2O_3 and γ-Fe_2O_3 phases in the film deposited at 1 mTorr. c) High resolution cross sectional TEM image of γ-Fe_2O_3 in α-Fe_2O_3 matrix.

existence of α-Fe_2O_3 and γ-Fe_2O_3 in the film. Furthermore, the γ-Fe_2O_3 phase in the present study showed several different orientation relationships with α-Fe_2O_3. This is probably due to the fact that PLD is a non-equilibrium growth technique.

The SAD pattern and the schematic in Figure 2b are from one of the Fe_2O_3 regions where α-Fe_2O_3 and γ-Fe_2O_3 coexist. The out-of-plane and the in-plane parameters of α-Fe_2O_3 as measured from the SAD patterns were $d(102) = 0.364$ nm and $d(1{-}12) = 0.370$ nm, respectively. The out-of-plane and the in-plane parameters in γ-Fe_2O_3 as measured from a high resolution TEM image (see Fig. 2c) were $d(120) = 0.37$ nm and $d(2{-}1{-}1) = 0.34$ nm, respectively, which are in good agreement with published values (i.e., JCPDS #39-1346). The lattice mismatch between α- and γ-Fe_2O_3 is 8.1 %. A distortion of the α-Fe_2O_3 lattice and strain concentration around γ-Fe_2O_3 was observed due to the large lattice mismatch.

The existence of secondary phases can affect the relaxation of misfit strain in $BiFeO_3$ and result in significant change in the ferroelectric and ferromagnetic properties of the $BiFeO_3$ film. To compare the relaxation mechanism of the out-of-plane lattice parameter of multiphase Bi-Fe-O with pure $BiFeO_3$, Bi-Fe-O films with a gradual change in thickness were fabricated by the gradient deposition technique using a shadow mask. An oxygen partial pressure of 20 mTorr was selected to fabricate a pure $BiFeO_3$ film, and 5 mTorr to make a multiphase Bi-Fe-O film. The thickness of these films varied in the range of 30–300 nm for pure $BiFeO_3$ and 30–290 nm for the multiphase Bi-Fe-O film. Figure 3a and b show a superposition of X-ray microdiffraction scans from different regions of the pure $BiFeO_3$ film (Fig. 3a) and multiphase Bi-Fe-O film (Fig. 3b) with different thicknesses. In Figure 3a, the position of the (002) peak of $BiFeO_3$ was found to shift from $2\theta = 44.6°$ to 45.6° as the film thickness increases. In contrast, the spectra in Figure 3b show a broad peak at $2\theta \approx 44.5°$ in the thin regions of the sample which evolves into two peaks as the film thickness increases; the thicker regions show a peak at ~45.7° which corresponds to $BiFeO_3$. However, a second peak at ~44.5° remains with weaker intensity even for thickness up to 300 nm. The observation of two peaks in Figure 3b is consistent with the coexistence of a strained region and a relaxed region in the film. More evidence of the two regions was obtained from TEM images as shown below. These results indicate that the multiphase film has a different relaxation mechanism than the pure $BiFeO_3$ films. Typically, the misfit strain between a film and a substrate is relaxed by the generation of misfit dislocations at the interface with increasing film thickness. As shown in Figure 3a, pure $BiFeO_3$ showed typical relaxation mechanisms in which the strain gradually relaxes as the film thickness increases (see Fig. 3c). The region in the multiphase Bi-Fe-O film with small thickness showed a highly strained film as expected. However, the thicker region of the film showed both a relaxed region (represented by the X-ray "peaks" labeled B in Figure 3b and a highly strained region (labeled A in Fig. 3b) in the film even though the thickness of the film was above the critical thickness for relaxation to take place. This observation can be explained by the formation of α-Fe_2O_3 regions, which appeared in the surface region of the film with thickness ≥50 nm. The transformation to α-Fe_2O_3 in the surface region of the film reduces the thickness of the $BiFeO_3$ underneath. Therefore, the area below α-Fe_2O_3 (marked A in Fig. 1b) showed higher misfit in-plane strain and a lower misfit dislocation density than the region with pure $BiFeO_3$ surrounding the α-Fe_2O_3 columns (marked B in Fig. 1b) as determined by high resolution TEM images (not shown). The formation of α-Fe_2O_3 regions enhances the relaxation of in-plane misfit strain in the $BiFeO_3$ columns between α-Fe_2O_3 columns due to the reduction in volume (calculated below). The reduction of volume releases both the in-plane compressive strain and out-of plane tensile strain in the $BiFeO_3$ regions surrounding α-Fe_2O_3 (see Fig. 3d).

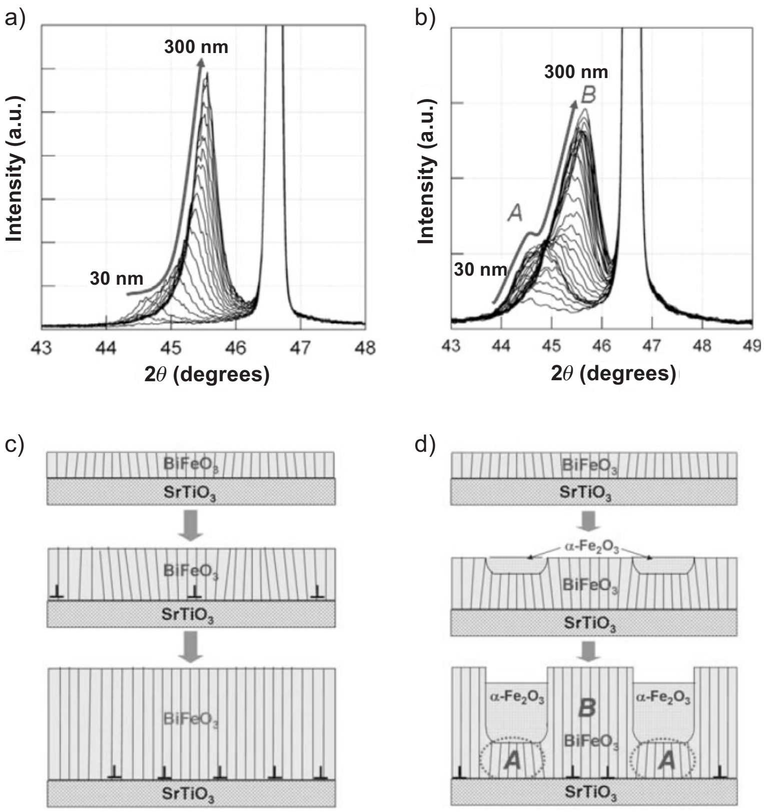

Figure 3. Superpositions of X-ray microdiffraction scans from regions of films with a thickness gradient grown at a) 20 mTorr and b) 5 mTorr. The thicknesses were varied from 30 to 300 nm. Schematics of the misfit strain relaxation mechanism in c) pure $BiFeO_3$ film and d) multiphase Bi-Fe-O film are suggested. Multiphase film shows coexistence of highly strained region (A) and relaxed region (B).

In order to determine if the strain relaxation mechanism of the multiphase film was due to the gradient in thickness, several multiphase Bi-Fe-O films, with constant thickness (35–500 nm), were grown and compared to the single phase $BiFeO_3$ film with a gradual change in thickness (see Fig. 4a). The change of out-of plane lattice parameter with thickness was obtained from the pure $BiFeO_3$ film with thickness gradient grown at 20 mTorr and the multiphase Bi-Fe-O films with constant thickness grown at 5 mTorr (see Fig. 4a). Both pure and multiphase films with 35 nm thickness showed a high degree of strain. As the film thickness increases from 30 to 300 nm, the out-of-plane lattice parameter of the pure $BiFeO_3$ film gradually decreases from 0.406 to 0.398 nm. However, in the multiphase films, the out-of-plane lattice parameter decreases from 0.407 to 0.396 nm with increasing film thickness from 35 to 500 nm. This result confirms that the α-Fe_2O_3 domains that form on the surface region of the film for films of thickness above 50 nm (grown at low oxygen partial pressure) enhance the in-plane relaxation of misfit strain in the $BiFeO_3$ columns. As a result, the total misfit strain reduction is from 0.51 % (pure $BiFeO_3$) to 0.25 % (mixture of $BiFeO_3$ and Fe_2O_3) at the thickness of ~300 nm. The observation of a broad peak in the XRD spectra in Figure 3b for thicknesses above ~50 nm indicates that the bottom portion of the films under the Fe_2O_3 region (region A) in Figure 1b remains strained. In order to understand the higher degree of stain relaxation in the films with Fe_2O_3, we estimate the change in volume in these regions. A reduction in volume of $\approx -19\,\%$ by the formation of the Fe_2O_3 phase allows expansion (in plane) of $BiFeO_3$ (which is under in-plane compressive strain with the substrate). This in-plane expansion, together with the formation of the vertical boundary between $BiFeO_3$ and Fe_2O_3, lower the out-of-plane strain in the film. Therefore, the formation of α-Fe_2O_3 by evaporation of the more volatile Bi metal at relatively low oxygen partial pressure enhances the relaxation of the compressive stress in $BiFeO_3$. The relaxation is accelerated as the α-Fe_2O_3 volume fraction increases.

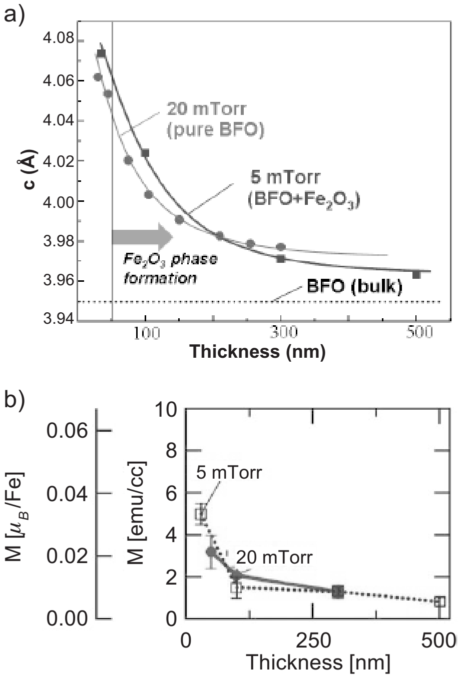

Figure 4. a) Out-of-plane lattice parameters in pure $BiFeO_3$ (thickness gradient) and $BiFeO_3$ with secondary phases (constant thickness) as a function of film thickness. b) Room temperature saturation magnetization (emu cm^{-3}) of Bi-Fe-O films as a function of thickness for films grown at 5 mTorr and 20 mTorr.

The existence of secondary phases also affects the magnetic properties of the films. We recently reported the dependence of the magnetic properties on the formation of Fe_2O_3 phases as controlled by the oxygen partial pressure during growth of Bi-Fe-O films.[15] The saturation magnetization increased to about 80 emu cm^{-3} due to the increase in the volume faction of γ-Fe_2O_3 in the film. In the present study, we compare the effect of strain and the formation of γ-Fe_2O_3 on the magnetization of $BiFeO_3$ films. α-Fe_2O_3 and $BiFeO_3$ are known as canted antiferromagnetic materials at room temperature, and they exhibit weak magnetization of 0.4 emu cm^{-3} and 2 emu cm^{-3} at room temperature, respectively.[21,22] In contrast, bulk γ-Fe_2O_3 is known to display magnetization of up to 400 emu cm^{-3} at room temperature.[23] In our previous study of $BiFeO_3$ films, the increase in volume of the γ-Fe_2O_3 with increasing film thickness showed a great effect on the magnetic properties of the films grown at less than 5 mTorr oxygen pressure.[15] However, the films grown at 5 mTorr oxygen pressure did not show dramatic increase in magnetization due to a small amount of γ-Fe_2O_3. The magnetization in this sample was controlled by residual strain in the film. Figure 4b shows the change in magnetization with thickness for films grown at 5 mTorr and 20 mTorr oxygen partial pressures. Both pure $BiFeO_3$ and multiphase Bi-Fe-O films exhibit higher magnetization for the thinner films than for thick films. From the XRD results in Figure 4a, the 35 nm thick film grown at 5 mTorr shows higher strain and higher magnetization (~5 emu cm^{-3}) (Fig. 4b) than the 50 nm thick $BiFeO_3$ film grown at 20 mTorr. However, the observed improvement of magnetization is still smaller than the results of Wang et al.,[5] but it is in agreement with other recent measurements.[13] This enhanced magnetism could result from the heteroepitaxial strain effect in the canted antiferromagnetic film. The magnetic moments of Fe in $BiFeO_3$ are ferromagnetically aligned on the (111) plane and antiferromagnetically switched along the [111] direction. Canting of Fe magnetic moment allows weak ferromagnetism in $BiFeO_3$.[24,25] Ederer and Spaldin found through density functional theory calculations that weak ferromagnetic moments ($0.1\,\mu_B$ per unit cell for about 1° canting from the collinear direction) are induced by a structural distortion.[26]

The $BiFeO_3$ in-plane lattice parameter, which is reduced by the compressive stress from the $SrTiO_3$ substrate, results in elongation of the out-of-plane lattice parameter. This strain gives rise to enhancement of magnetization.[5,13] As the thickness increases, this strain is relaxed and the magnetization is expected to decrease. Since the multiphase $BiFeO_3$ films have higher strain relaxation due to the formation of α-Fe_2O_3 domains, the magnetization in these films is expected to decrease faster than for pure $BiFeO_3$ films with increasing thickness. However, this reduction of magnetization is partially compensated by the nucleation of γ-Fe_2O_3. The saturation magnetization decreases with increasing oxygen partial pressure up to 20 mTorr and remains constant above this pressure when the films become pure $BiFeO_3$.

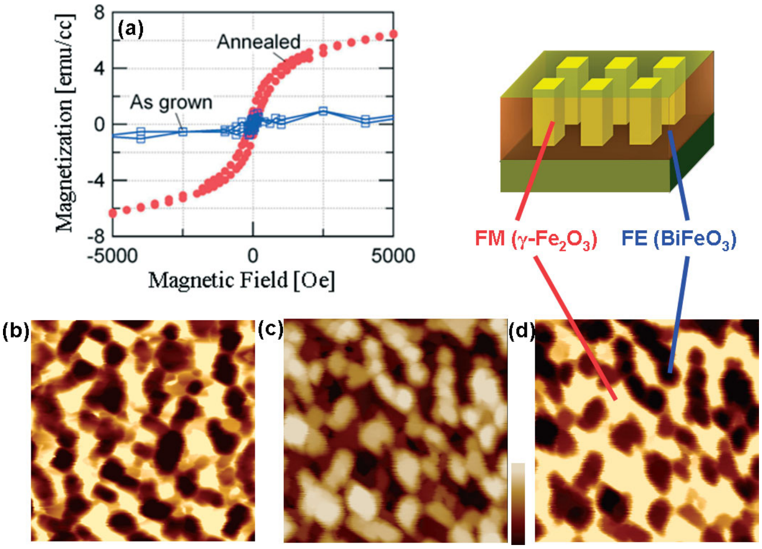

Figure 5. a) Hysteresis loops of as grown and annealed multiphase Bi-Fe-O films. c) AFM topographic image and b) and d) magnetic force microscopy images of an annealed multiphase film with no external field and after magnetizing the film perpendicular to the surface by applying 20 kOe magnetic field, respectively. AFM and MFM images are 4 × 4 µm scans. The height scale in (c) corresponds to 0–100 nm. The higher (brighter) regions are the $BiFeO_3$ phase. Schematic is the microstructure of Bi-Fe-O multiferroic nanocomposites.

To further enhance the magnetic properties of multiphase Bi-Fe-O film with the columnar structure, we explored the possibility of transforming the α-Fe_2O_3 (antiferromagnetic phase) regions to γ-Fe_2O_3 (ferromagnetic phase).[27] We have devised a two-step process for this purpose. The first stage is hydrogen reduction to transform α-Fe_2O_3 into Fe_3O_4, and the second stage is oxidation to transform Fe_3O_4 to γ-Fe_2O_3. The reduction was conducted by flowing a mixture gas of Ar and H_2 (10_{Ar}:1_{H2}) for 1 hour while the film was kept at 300 °C. This was followed by oxidization at 300 °C in oxygen ambient for 1 hour. The change of magnetization after the annealing process is shown in Figure 5a. The annealed film showed increased magnetization (~ 6 emu cm^{-3}) due to the increase of the γ-Fe_2O_3 fraction (less than 10 %). The magnetic domain image of the annealed multiphase Bi-Fe-O film was acquired using MFM to confirm the existence of magnetic domains (γ-Fe_2O_3) after annealing. Figure 5b shows randomly oriented magnetic domains with zero field that switch in the perpendicular direction under an applied magnetic field (Fig. 5d). Comparing the AFM image in Figure 5c with the MFM image in Figure 5d, we can see that the magnetic domains in the films correspond to the Fe_2O_3 regions. From these results, we conclude that the magnetic properties of the films can be controlled by converting α-Fe_2O_3 into γ-Fe_2O_3 through the described procedure. In fact, we found that the magnetization of the films is directly proportional to the volume fraction of γ-Fe_2O_3 which can be controlled by adjusting the annealing time and the concentration of hydrogen in the gas mixture.

Also, effects of the Fe_2O_3 phase formation and microstructural change on the ferroelectric properties of $BiFeO_3$ films were studied using piezo force microscopy (PFM). Figure 6a and b show a topographic image and an out-of-plane piezoelectric response image, respectively, of a multiphase $BiFeO_3$ thin film obtained using PFM at room temperature. Figure 6a shows a columnar structure of $BiFeO_3$ and Fe_2O_3. Relatively high regions represent $BiFeO_3$. To obtain the piezoelectric response image, the multiphase $BiFeO_3$ film (Fig. 6b) and pure $BiFeO_3$ film (Fig. 6c) were first poled by applying a positive DC bias (+10 V) to a conducting probe while scanning over a 3 × 3 µm^2 area. Another poling was then performed with a negative voltage (–10 V) during a scan over a 1 × 1 µm^2 area. The PFM image shows both written regions with opposite contrast because of the presence of switching of ferroelectric domains in the film. Comparing switching of domains in the pure $BiFeO_3$ film (Fig. 6c) to the multiphase $BiFeO_3$ film (Fig. 6b), the multiphase $BiFeO_3$ film shows enhanced piezo electric response with higher contrast of switching in polarization in the interfacial regions between $BiFeO_3$ and Fe_2O_3 than the pure $BiFeO_3$ film. This result is surprising because Fe_2O_3 is not ferroelectric. It is possible that local strains and/or composition gradients across these interfacial regions are responsible for the enhanced piezo electric response. These possibilities are currently under further investigation.

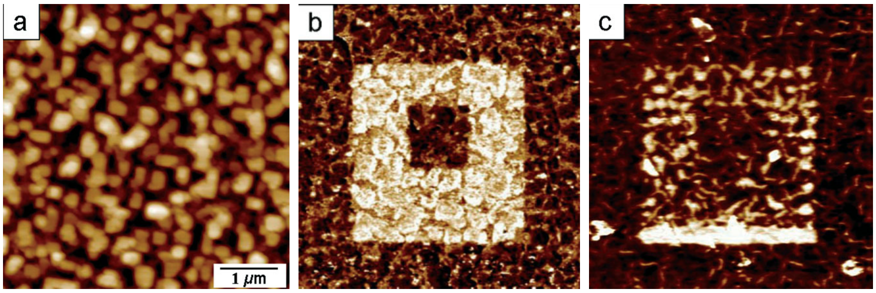

Figure 6. a) AFM topographic image and b) PFM image of ferroelectric domains in multiphase $BiFeO_3$ and c) PFM image of ferroelectric domains in pure $BiFeO_3$. A DC bias of +10 V was applied within 3 × 3 µm^2 area, and then –10 V was applied within 1 × 1 µm^2 area in the piezo force microscopy images.

In conclusion, pure $BiFeO_3$ films were grown on $SrTiO_3$ with 20 mTorr oxygen pressure. At oxygen pressures below or equal to 5 mTorr, regions containing α-Fe_2O_3 and γ-Fe_2O_3 appear on the top region of the film when the thickness of the film is ~ 50 nm. With continuous deposition, these Fe_2O_3 regions continue to grow to the surface of the film. γ-Fe_2O_3 nucleates in α-Fe_2O_3 with specific orientation forming plate-like structures. The distribution of misfit strain in multiphase Bi-Fe-O film was compared to pure BiFeO$_3$ film, and a strain relaxation mechanism was suggested. The formation of α-Fe$_2$O$_3$ prevented the relaxation of the misfit strain in the BiFeO$_3$ regions below α-Fe$_2$O$_3$ columns. The α-Fe$_2$O$_3$, however, assisted in the relaxation of strain in the BiFeO$_3$ columns between α-Fe$_2$O$_3$. Preliminary studies show that this misfit strain accommodation caused by formation of α-Fe$_2$O$_3$ significantly enhances the piezo electric properties ($d_{33} \simeq 70$ pm V^{-1}) and electrical polarization of BiFeO3 which increased from ~2 to 70 μC cm^{-2} (these results will be reported elsewhere).

The magnetization of Bi-Fe-O films is slightly (~5 emu cm^{-3}) enhanced by strain. However, the large increase in magnetization (of up to ~80 emu cm^{-3}) in BiFeO$_3$ films is directly proportional to the volume fraction of γ-Fe$_2$O$_3$. We also demonstrated that transformation of α-Fe$_2$O$_3$ to γ-Fe$_2$O$_3$ is possible by a reduction and oxidation process. This process can be used to increase the magnetization in Bi-Fe-O films. Our results show the possibility of tuning the microstructure and the fraction of the three phases in the Bi-Fe-O system. We have demonstrated that multiferroic nanocomposites with separated columnar structure of ferroelectric and ferromagnetic domains can be achieved by controlling the deposition oxygen pressure, and the properties of the magnetic domains can be tailored to applications through an annealing procedure.

Experimental

Bi-Fe-O thin films with constant thickness (35–500 nm) and with a thickness gradient were deposited on SrTiO$_3$ (001) substrates at a temperature of 650 °C by PLD. We ablated a stoichiometric BiFeO$_3$ target with a KrF excimer laser ($\lambda = 248$ nm) with a typical fluence of 2 J cm^{-2}. The substrates were preheated to 650 °C before deposition, and the deposition rate was ≈ 6 nm min^{-1}. To investigate the multiphase formation, the oxygen partial pressure was varied in the range of 0.1 to 20 mTorr. We also examined the evolution of the crystal structure in films as a function of thickness ranging from 35 to 500 nm, all grown at a constant oxygen partial pressure (5 mTorr). Scanning X-ray microdiffraction (using a D8 DISCOVER with GADDS for combinatorial screening by Bruker-AXS), and EDAX energy dispersive X-ray spectroscopy (EDS) in a JEOL 2010F field emission transmission electron microscope (TEM) were used for identifying the secondary phases. The structural properties of the films were studied by TEM. TEM images and selected area diffraction (SAD) patterns of the films were obtained with a JEOL 4000-FX TEM operated at an accelerating voltage of 300 KV and a JEOL 2100F field emission TEM operated at an accelerating voltage of 200 KV. A MPMS-5 superconducting quantum interference device (SQUID) magnetometer and Digital Instruments (DI) Dimensions 3000 magnetic force microscopy (MFM) were used to perform magnetic characterization. PFM was performed in contact mode on BiFeO$_3$/Nb-doped SrTiO$_3$ structures using Pt-Ir coated tips [28].

Received: January 13, 2007
Revised: May 16, 2007

[1] G. A. Smolenskii, I. E. Chupis, *Sov. Phys. Usp.* **1982**, *25*, 475.
[2] S. Alexander, S. Shtrikman, *Solid State Commun.* **1966**, *4*, 115.
[3] E. Fischer, G. Gorodetsky, R. M. Hornreich, *Solid State Commun.* **1972**, *10*, 1127.
[4] T. Kimura, T. Goto, H. Shintani, K. Ishizaka, T. Arima, Y. Tokura, *Nature* **2003**, *426*, 55.
[5] J. Wang, J. B. Neaton, H. Zheng, V. Nagarajan, S. B. Ogale, B. Liu, D. Viehland, V. Vaithyanathan, D. G. Schlom, U. V. Waghmare, N. A. Spaldin, K. M. Rabe, M. Wuttig, R. Ramesh, *Science* **2003**, *299*, 1719.
[6] N. Hur, S. Park, P. A. Sharma, J. S. Ahn, S. Guha, S.-W. Cheong, *Nature* **2004**, *429*, 392.
[7] M. Fiebig, T. Lottermoser, D. Fröhlich, A. V. Goltsev, R. V. Pisarev, *Nature* **2002**, *419*, 818.
[8] Z. J. Huang, Y. Cao, Y. Y. Sun, Y. Y. Xue, C. W. Chu, *Phys. Rev. B* **1997**, *56*, 2623.
[9] M. Murakami, S. Fujino, S.-H. Lim, C. J. Long, L. G. Salamanca-Riba, M. Wuttig, I. Takeuchi, V. Nagarajan, A. Varatharajan, *Appl. Phys. Lett.* **2006**, *88*, 162 902.
[10] V. A. Murashav, D. N. Rakov, V. M. Ionov, I. S. Dubenko, Y. U. Titov, *Ferroelectrics* **1994**, *162*, 11.
[11] Y. F. Popov, A. M. Kadomtseva, G. P. Vorobev, A. K. Zvezdin, *Ferroelectrics* **1994**, *162*, 135.
[12] W. M. Zhu, Z.-G. Ye, *Ceram. Int.* **2004**, *30*, 7, 1435.
[13] W. Eerenstein, F. D. Morrison, J. Dho, M. G. Blamire, J. F. Scott, N. D. Mathur, *Science* **2005**, *307*, 1203a.
[14] H. Béa, M. Bibes, A. Barthélémy, K. Bouzehouane, E. Jacquet, A. Khodan, J.-P. Contour, S. Wyczisk, A. Forget, D. Lebeugle, D. Colson, M. Viert, *Appl. Phys. Lett.* **2005**, *87*, 072 508.
[15] M. Murakami, S. Fujino, S.-H. Lim, L. G. Salamanca-Riba, M. Wuttig, I. Takeuchi, H. Sugaya, T. Hasegawa, S. E. Lodland, *Appl. Phys. Lett.* **2006**, *88*, 112 505.
[16] G. M. Meyer, R. J. Nelmes, J. Hutton, *Ferroelectrics* **1978**, *21*, 461.
[17] JCPDS Card numbers 33-0664, 39-1346.
[18] S. Kachi, K. Momiyama, S. Shimizu, *J. Phys. Soc. Jpn.* **1963**, *18*, 106.
[19] M. T. Johnson, J. R. Michael, S. R. Gilliss, C. B. Carter, *Philos. Mag. A* **1999**, *79*, 2887.
[20] J. D. Bernal, D. R. Dasgupta, A. L. Mackay, *Nature* **1957**, *180*, 645.
[21] Y.-Y. Li, *Phys. Rev.* **1956**, *101*, 1450.
[22] K. Y. Yun, M. Noda, M. Okuyama, H. Seki, H. Tabata, K. Saito, *J. Appl. Phys.* **2004**, *96*, 3399.
[23] A. J. Koch, J. J. Becker, A. E. Berkowitz, W. J. Schuele, P. J. Flanders, *J. Appl. Phys.* **1968**, *39*, 1261.
[24] I. E. Dzyaloshinskii, *Sov. Phys. JETP* **1957**, *5*, 1259.
[25] T. Moriya, *Phys. Rev.* **1960**, *120*, 91.
[26] C. Ederer, N. A. Spaldin, *Phys. Rev. B* **2005**, *71*, 060 401.
[27] B. J. Kim, E. T. Lee, G. E. Jang, *Thin Solid Films* **1999**, *341*, 79.
[28] V. Nagarajan, A. Stanishevsky, L. Chen, T. Zhao, B.-T. Liu, J. Melngailis, A. L. Roytburd, J. Finder, Z. Yu, R. Droopad, K. Eisenbeiser, R. Ramesh, *Appl. Phys. Lett.* **2002**, *81*, 4215.